TRIGGERING FREEZE/THAW SURFACE STATE MONITORING FROM HIGH INCLINATION ORBIT GNSS-R MISSIONS: A CYGNSS-BASED STUDY

Hugo Carreno-Luengo and Christopher S. Ruf

Climate and Space Sciences and Engineering Department, University of Michigan (UMich)
Ann Arbor, MI, United States of America (USA)
Email: {carreno,cruf}@umich.edu

IGARSS 2022 - 2022 IEEE International Geoscience and Remote Sensing Symposium | 978-1-6654-2792-0/22/$31.00 ©2022 IEEE | DOI: 10.1109/IGARSS46834.2022.9883093

ABSTRACT

NASA's Cyclone Global Navigation Satellite System (CYGNSS) mission has been in orbit for more than 5 years. Following the Earth Science Division 2020 Senior Review, NASA announced last year it is extending the CYGNSS mission through at least 30th September 2023. The extended CYGNSS mission phase will focus on both ocean and land surface scientific investigations. One new recent application of CYGNSS is Freeze/Thaw (F/T) surface state detection and imaging [1]. The main objective of this presentation is the application of the retrieval algorithm developed in [1] over different high-interest target areas within the CYGNSS coverage to show the capability to provide long-term trending of F/T behaviour.

Index Terms— CYGNSS, GNSS-R, Freeze/Thaw

1. INTRODUCTION

F/T surface state monitoring is important for quantifying carbon, energy, and water fluxes, and their impact on land cover change [2-4]. At present, there is a lack of operational spaceborne measurements of active layer thickness. In this study, we analyze F/T surface state changes due to water-ice phase conversion. These changes are an indirect measurement of active layer thickness.

CYGNSS Earth Venture mission is an 8-microsatellites single-plane GNSS-R constellation [5,6]. It uses the cGNSS-R technique [7], which consists of the direct correlation of the reflected signal with a locally generated replica of the transmitted one (GPS L1 C/A). The down-looking antenna is Left Hand Circular Polarized (LHCP) and the gain at the boresight is ~ 14.5 dB.

CYGNSS is a science-driven Earth exploration mission. The continuous and dynamic evolution of the CYGNSS data products available through the Physical Oceanography Distributed Active Archive Center [8] is fostering innovative research and enhanced application areas.

Some few F/T studies were performed using GNSS-R [1,9-13]. In this study, we demonstrate the capabilities of GNSS-R for F/T retrieval and monitoring. Section 2 shows an overview of the methodology, Section 3 presents the results, and the preliminary conclusions are highlighted in Section 4. While CYGNSS operates in a low inclination orbit, the *know-how* developed here could be used in future high-inclination GNSS-R missions.

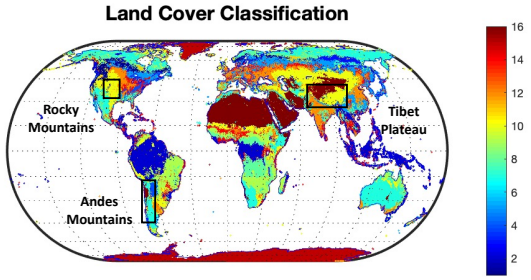

Fig. 1. Target areas located over a global International Geosphere-Biosphere Program (IGBP) land cover classification map derived from Moderate-Resolution Imaging Spectroradiometer (MODIS): 1 (Evergreen needleleaf forest), 2 (Evergreen broadleaf forest), 3 (Deciduous needleleaf forest), 4 (Deciduous broadleaf forest), 5 (Mixed forest), 6 (Closed shrublands), 7 (Open shrublands), 8 (Woody savannas), 9 (Savannas), 10 (Grassland), 11 (Permanent wetlands), 12 (Croplands), 13 (Urban and built-up), 14 (Cropland/Natural veg. mosaic), 15 (Snow and ice), 16 (Barren or sparsely vegetated).

2. METHODOLOGY

2.1 Fundamental Observable

The fundamental observable used in this study is the CYGNSS v3.0 power Delay Doppler Map (DDM) after radiometric calibration. Power DDMs are the true power as measured by an ideal analog sensor without additional postprocessing. This selection enables a more accurate and focused estimation of the surface reflectivity than using data products such as e.g. the signal-to-noise ratio or processed observables such as e.g. the Normalized Bistatic Radar Cross Section (NBRCS), which depend on external algorithms and scattering assumptions.

2.2 Metadata and Quality Flags

CYGNSS products are dynamically improving in performance and are increasing the number of available metadata and quality flags. In this study, the following metadata are used: a) transmitter Equivalent Isotropically Radiated Power (EIRP), b) antenna gain, c) distance between each CYGNSS spacecraft and the nominal specular point, d) distance between each GPS satellite and the nominal specular point, e) geographical coordinates of

the nominal specular point. The equivalent overall quality flag over land surfaces is applied to select the highest-quality dataset.

2.3 Processed Observable

Final DDMs are obtained after the interpolation of the improved 1700 x 1100 bins DDMs. In so doing, a spline method is used. This improves the quality of the original 17 x 11 bins fundamental DDMs. This improvement is implemented to partially mitigate the potential impact of topography in the tracking of the peak of the DDMs, which is used for the estimation of the surface reflectivity.

2.4 Reflectivity

The reflectivity is estimated based on the procedure described in [1]. There is a relationship between the reflectivity and the Fresnel reflection coefficient, which depends on the surface permittivity. When the soil surface changes from frozen to thawed, the permittivity increases. The ability of CYGNSS to estimate the reflectivity is high because of the strong sensitivity of L-band GNSS signals to the permittivity, which depends on the phase of the water, and because of the higher biomass penetration depth as compared to higher frequencies.

2.5 Surface Gridding Strategy

CYGNSS surface sampling properties are pseudo-random. Surface gridding and a spatio-temporal averaging strategies are needed to generate continuous land surface spatial information. The size of the grid is a trade-off between the required spatial resolution for the study of a specific surface variable (soil moisture, biomass, inland waters …) and the temporal resolution associated with the dynamics of the specific variable. The temporal resolution depends on the CYGNSS revisit time. The size of the grid should account for the available number of CYGNSS measurements within the required time interval.

Additionally, a smoothing approach should be considered to account for the pseudo-random nature of the surface sampling and the impact of the incidence angle on the spatial resolution of each individual CYGNSS measurement.

In this study, a 0.1° x 0.1 ° grid is used and a moving-averaging filter of 0.1 ° x 0.1 ° is applied at steps of 0.1 °. The rationale behind this selection is to increase the number of measurements per pixel so as to generate a statistically significant population. Additionally, with this respect, the temporal averaging is set to 1 month to enable the required number of measurements and because this is a long-term study focused on the yearly evolution of the F/T cycle. Because of the pseudo-random sampling properties, the grid size is larger than in [1], to reduce the differences between the 3 different target areas.

2.6 Seasonal Threshold Algorithm

The retrievals are based on our recent F/T seasonal-threshold algorithm [1]. This algorithm evaluates the relationship between time series of CYGNSS-derived reflectivity Γ and seasonal reference frozen and thawed

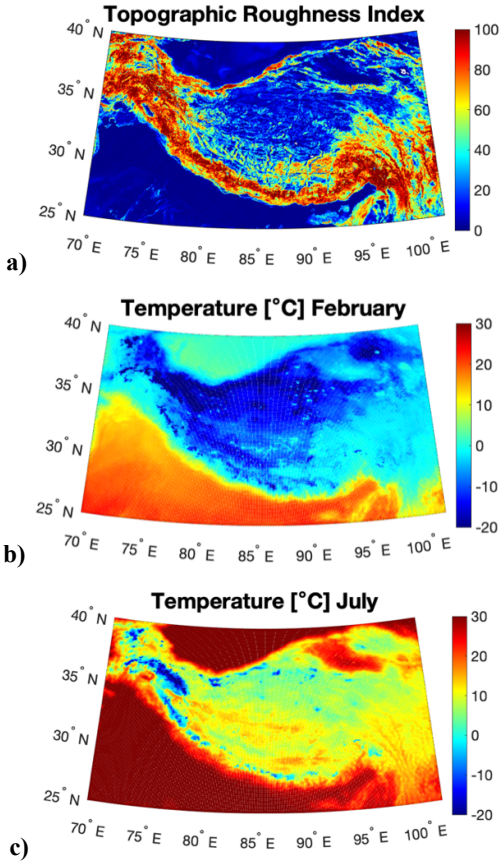

Fig. 2. This target area is the Tibet Plateau (Lat = [25 40] °, Lon = [70 110] °). Auxiliary information: a) Topographic Roughness Index (TRI), b) ERA5-Land surface temperature February 2019, c) ERA5-Land surface temperature July 2019.

states. For a measurement at time t, the seasonal scale factor $\Delta(t)$ is defined as follows:

$$\Delta(t) = \frac{\Gamma(t) - \Gamma_{fr}}{\Gamma_{th} - \Gamma_{fr}} \quad (1)$$

where $\Gamma(t)$ is the reflectivity measurement estimated at time t, and Γ_{fr} & Γ_{th} are reflectivity measurements corresponding to frozen and thawed reference states, respectively. The frozen and thawed references states are calculated as the 10 % and the 90 % points in the Cumulative Distribution Function (CDF) of the reflectivity at each pixel. Different F/T surface states correspond to different observation times.

3. FIRST RESULTS

The Tibet Plateau is selected to illustrate first results here. The dominant IGBP land cover types are grassland, barren, and shrublands (Fig. 1). The TRI is high (> 70) over the Himalayan Mountains and low (< 20) over the central part of the Tibet Plateau (Fig. 2a). The European Centre for Medium-Range Weather Forecast (ECMWF) ERA5-land surface temperatures are also shown for Winter (Fig. 2b)

a1) 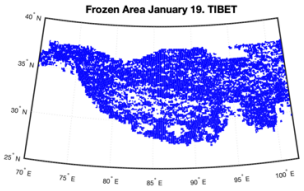

b1) 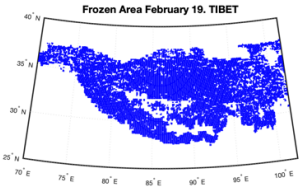

c1) 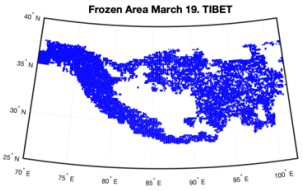

d1) 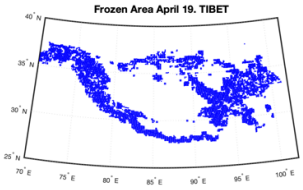

e1) 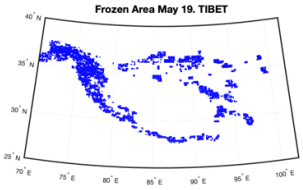

f1) 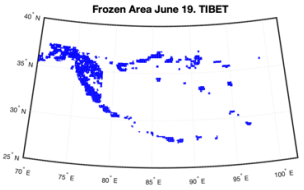

g1) 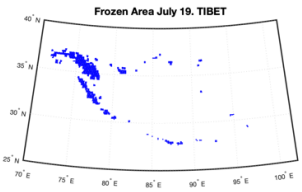

h1) 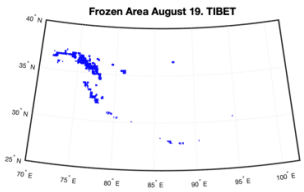

i1) 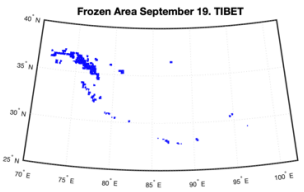

j1) 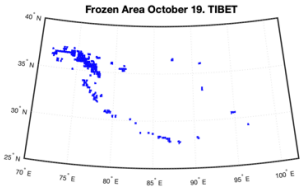

k1) 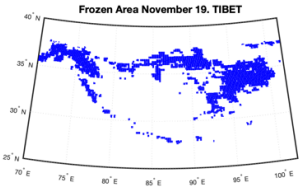

l1) 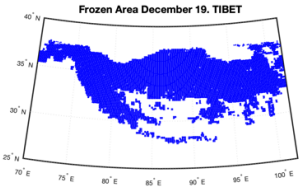

a2) 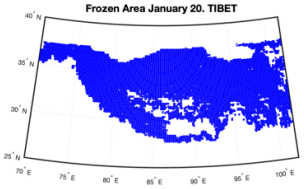

b2) 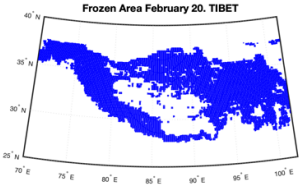

c2) 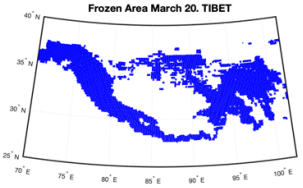

d2) 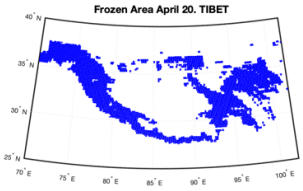

e2) 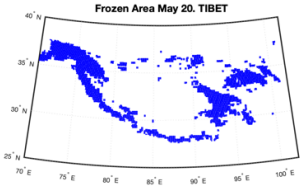

f2) 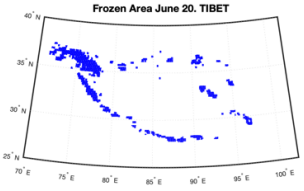

g2) 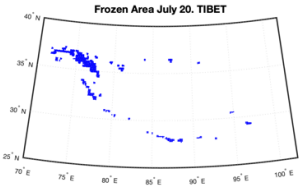

h2) 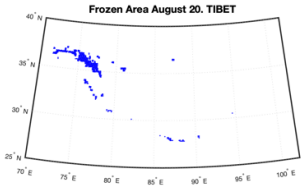

i2) 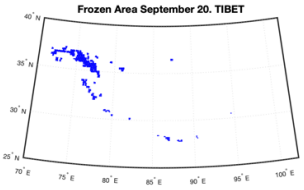

j2) 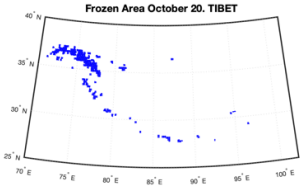

k2) 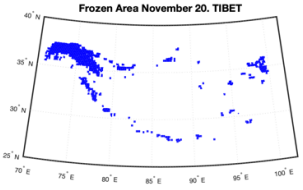

l2) 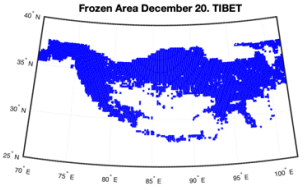

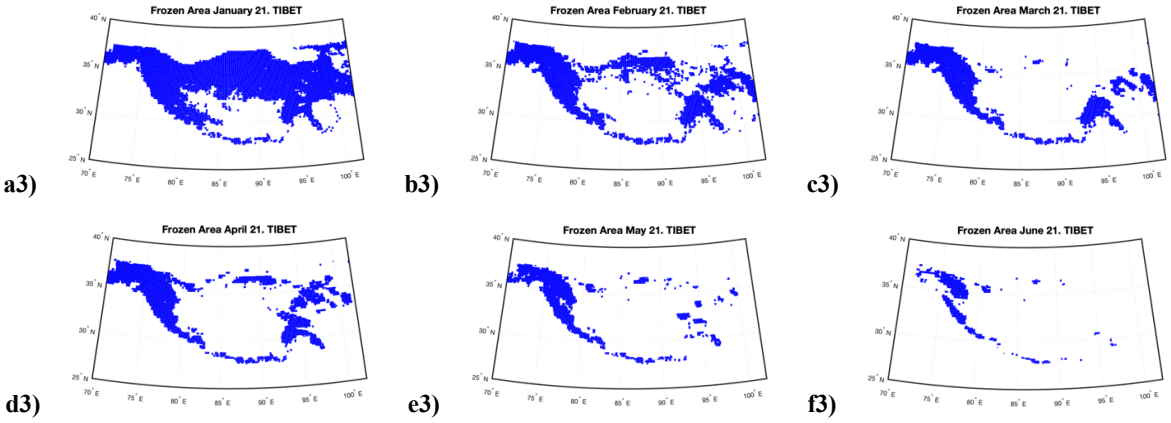

Fig. 3. CYGNSS-derived temporal evolution of the frozen area extend over the Tibet Plateau from January 2019 to June 2021.

and Summer (Fig. 2c). There is a strong temperature gradient between both seasons, with extended permafrost areas.

Fig. 3 shows the temporal monthly-evolution of the CYGNSS-derived frozen area from January 2019 to June 2021. There is a clear spatial pattern corresponding to surface features of the Tibet Plateau. The temporal evolution shows a reasonable trend from Winter to Summer with a remaining frozen area in Summer, over the Himalayas Mountains, which corresponds to a permafrost area.

4. CONCLUSIONS

Soil F/T transition monitoring is essential for quantifying climate change and hydrologic dynamics over cold regions. The F/T changes of seasonally frozen ground are an important indicator of climate change and contributor to global methane distributions. Our F/T seasonal threshold algorihm is aplied to 30 months of CYGNSS data over 3 different high-altitude target areas. First results are shown here over the Tibet Plateau. This work demonstrates the capability of long-term monitoring of F/T surface state at a global scale. Future high-inclination orbit GNSS-R missions e.g. [14] will enable the application of this retrieval algorithm over higher latitude regions. The higher spatio-temporal sampling of GNSS-R as compared to more traditional Remote Sensing techniques could open new insights in monitoring highly dynamic F/T surfaces processes.

5. REFERENCES

[1] H. Carreno-Luengo and C. Ruf, “Retrieving Freeze/Thaw Surface State from CYGNSS Measurements,” IEEE Transactions on Geoscience and Remote Sensing, vol. 60, no. 4302313, pp. 1-13, Oct. 2021.

[2] B. P. Selvam, H. Laudon, F. Guillemette, and M. Berggren, “Influence of Soil Frost on the Character and Degradability of Dissolved Organic Carbon in Boreal Forest Soils,” AGU Journal Geophysical Research, Biogeoscience, vol. 121, no. 3, pp. 829-840, Mar. 2016.

[3] M. L. Goulden et al., “Sensitivity of Boreal Forest Carbon Balance to Soil Thaw,” Science, vol. 279, no. 5348, pp. 214-217, Jan. 1998.

[4] L. Øygarden, “Rill and Gully Development During an Extreme Winter Runoff Event in Norway,” CATENA, vol. 50, no. 2-4, pp. 217-242, Jan. 2003.

[5] C. Ruf, et al., "CYGNSS Handbook," Ann Arbor, MI, Michigan Pub., ISBN 978-1-60785-380-0, Apr. 2016.

[6] H. Carreno-Luengo, J.A. Crespo, R. Akbar, A. Bringer, A. Warnock, M. Morris, and C. Ruf, “The CYGNSS Mission: On-Going Science Team Investigations,” MDPI Remote Sensing, vol. 13, no. 9, pp. 1814, May 2021.

[7] H. Carreno-Luengo, A. Camps, N. Floury, M. Martin-Neira, C. Ruf, T. Wang, S.J. Khalsa, M.P. Clarizia, J. Reynolds, J. Johnson, A. O’Brien, C. Galdi, M. di Bisceglie, A. Dielacher, P. Jales, M. Unwin, L. King, G. Foti, R. Shah, D. Pascual, B. Schreiner, M. Asgarimehr, J. Wickert, S. Ribo, and E. Cardellach, “The IEEE-SA Working Group on Spaceborne GNSS-R: Scene Study,” IEEE Access, vol. 9, pp. 89906-89933, Jun. 2021.

[8] Physical Oceanography Distributed Active Archive Center. [Online]. Available: https://podaac.jpl.nasa.gov/ (10 May 2022)

[9] H. Carreno-Luengo, S. Lowe, C. Zuffada, S. Esterhuizen, and S. Oveisgharan, “Spaceborne GNSS-R from the SMAP mission: First Assessment of Polarimetric Scatterometry over Land and Cryosphere,” MDPI Remote Sensing, vol. 9, no. 4, pp. 362, Apr. 2017.

[10] C. Chew, S. Lowe, N. Parazoo, S. Esterhuizen, S. Oveisgharan, E. Podest, C. Zuffada, and A. Freedman, “SMAP Radar Receiver Measures Land Surface Freeze/Thaw State Through Capture of Forward-Scattered L-Band Signals,” Remote Sensing of Environment, vol. 198, pp. 333-344, Sep. 2017.

[11] D. Comite, L. Cenci, A. Colliander, and N. Pierdicca, “Monitoring Freeze-Thaw State by Means of GNSS Reflectometry: An Analysis of TechDemoSat-1 Data,” IEEE Journal of Selected Topics in Applied Earth Observations and Remote Sensing, vol. 13, pp. 2996-3005, May 2020.

[12] X. Wu, Z. Dong, S. Jin, Y. He, Y. Song, W. Ma, and L. Yang, “First Measurement of Soil Freeze/Thaw Cycles in the Tibetan Plateau Using CYGNSS GNSS-R Data,” MDPI Remote Sensing, vol. 12, no. 15, pp. 2361, Jul. 2020.

[13] K. Rautiainen, D. Comite, J. Cohen, E. Cardellach, M. Unwin, and N. Pierdicca, “Freeze-Thaw Detection over High-Latitude Regions by Means of GNSS-R Data,” IEEE Transactions on Geoscience and Remote Sensing, vol. 60, no. 4302713, pp. 1-13, Nov. 2021.

[14] M. Unwin, N. Pierdicca, E. Cardellach, K. Rautiainen, G. Foti, P. Blunt, L. Guerriero, E. Santi, and M. Tossaint, “An Introduction to the HydroGNSS GNSS Reflectometry Remote Sensing Mission,” IEEE Journal of Selected Topics in Applied Earth Observations and Remote Sensing, vol. 14, no. 6987-6999, pp. 6987-6999, Jun. 2021.

Acknowledgements

This research was supported in part by the NASA Science Mission Directorate contract 80LARC21DA003 with the University of Michigan.